AIAA JOURNAL
Vol. 34, No. 8, August 1996

Low-Reynolds-Number Separation on an Airfoil

J. C. Muti Lin* and Laura L. Pauley†
Pennsylvania State University, University Park, Pennsylvania 16802-1412

Unsteady boundary-layer separation from an Eppler 387 airfoil at low Reynolds number is studied numerically. Through a series of computations, the effects of Reynolds number and angle of attack are investigated. For all cases, vortex shedding is observed from the separated shear layer. From linear stability analysis, a Kelvin–Helmholtz instability is identified as causing shear layer unsteadiness. The low-turbulence wind-tunnel tests of the Eppler 387 airfoil are used to compare with the time-averaged results of the present unsteady computations. The favorable comparison between computational and experimental results strongly suggests that the unsteady large-scale structure controls the low-Reynolds-number separation bubble reattachment with small-scale turbulence playing a secondary role.

Nomenclature

C = chord length
C_D = drag coefficient
C_L = lift coefficient
C_P = pressure coefficient
f = shedding frequency
Re = chord Reynolds number
RP = reattachment point
SP = separation point
Sr = Strouhal number
U = velocity
θ = momentum thickness

Subscripts

sep = conditions at separation
∞ = freestream conditions

I. Introduction

LOW-REYNOLDS-NUMBER aerodynamics is important for both military and civilian applications. These applications include propellers, remotely piloted vehicles, sailplanes, ultralight man-carrying/man-powered aircrafts, leading-edge control devices, high-altitude vehicles, and wind turbines. Since three-dimensionality is typically important only near the foil tip, flow about two-dimensional cross sections has been the focus of much research in low-Reynolds-number aerodynamics.[1–5]

The low-Reynolds-number separation bubble can extend across 15% of the airfoil surface.[6] Hence accurate prediction of its existence and extent is necessary in the design of efficient low-speed airfoils. The conventional time-averaged model of the laminar separation bubble, sketched by Horton,[7] is shown in Fig. 1. Distinguishing characteristics of this laminar separation bubble are the regions of nearly uniform static pressure downstream of the separation point and the abrupt rise in pressure near the reattachment point. Flow visualization and hot-wire studies of Brendel and Mueller[8] and LeBlanc et al.[9] demonstrate an essentially steady, stagnant flow within the dead air region beyond the separation point. In this region, the shear layer lifts slowly from the surface. Beyond the transition point the strongly recirculating flow is unsteady and the shear layer reattaches shortly downstream. The unsteady region of the separation bubble is often described as being turbulent. Experimental and computational studies, however, have found that the velocity fluctuations are primarily the result of a low-frequency oscillation a characteristic of vortex shedding.

When the local Reynolds number based on boundary-layer quantities is sufficiently high, the natural transition of an attached boundary layer is caused by the amplification of Tollmien–Schlichting (viscous-type) instabilities. However, in the low-Reynolds-number regime ($Re < 5 \times 10^5$), this viscous-type transition would occur only when boundary-layer tripping is applied. If the boundary layer separates, Kelvin–Helmholtz (inviscid-type) instabilities will develop as a result of the separated inflectional velocity profile. Since Kelvin–Helmholtz instabilities cause the shear layer to roll up, it might be expected that the unsteadiness in the separation bubble will be dominated by large-scale vortex shedding and not small-scale turbulence.

Previous studies[10,11] computationally investigated the characteristics of a separation bubble generated on a flat plate with adverse pressure gradient. Vortex shedding was observed as the primary flow unsteadiness. The present study considers the separation from the curved surface of an airfoil to determine the universality of the previous numerical findings concerning the unsteady large-scale structure in low-Reynolds-number separation. The underlying dominant instability mechanism causing vortex shedding is also identified. The effects of Reynolds numbers and angle of attack on the evolution of the unsteady separated flow are systematically investigated. Finally, the validity of the current unsteady approach is evaluated by time averaging the computational results and comparing with inherently time-averaged experimental measurements. The Eppler 387 airfoil was chosen because of the importance of an airfoil geometry to most lifting devices and the availability of detailed experimental measurements.[12]

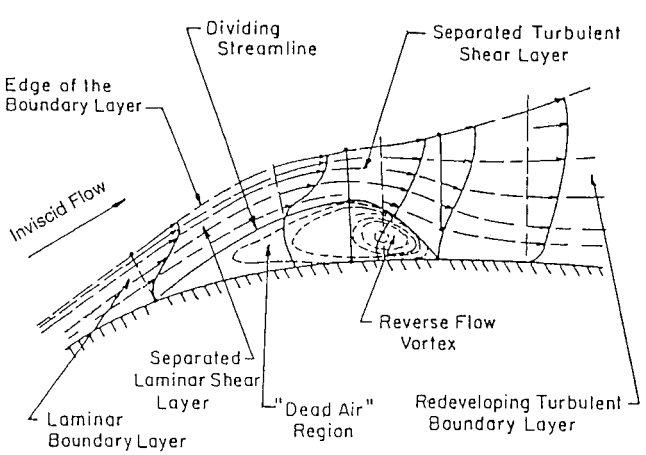

Fig. 1 Phenomenological features of a laminar separation bubble.[7]

Received July 14, 1993; revision received Feb. 1, 1996; accepted for publication Feb. 29, 1996.

*Research Assistant, Department of Mechanical Engineering.
†Associate Professor, Department of Mechanical Engineering. Member AIAA.

II. Background

McGhee et al.[12] conducted tests in the Langley Low-Turbulence Pressure Tunnel to determine the performance characteristics of the Eppler 387 airfoil at Reynolds numbers from 6×10^4 to 4.6×10^5. Pressure measurements were used to obtain lift and pitch moment, whereas wake surveys were used to determine airfoil drag. Oil-flow visualization identified the locations of laminar separation and reattachment. They concluded that the performance of this airfoil is dominated by the presence of a laminar separation bubble at Reynolds number below 2×10^5. An energetic low-frequency oscillation was measurable and caused the reattachment point to move back and forth for Reynolds number of 6×10^4. The primary focus of McGhee et al. was the time-averaged structure of the separation bubble. However, the measured low-frequency oscillation at $Re = 6 \times 10^4$ clearly suggests a large-scale unsteady phenomena.

Other experimental investigations also found a low-frequency oscillation of the laminar separation bubble near the reattachment point. LeBlanc et al.[9] made unsteady velocity measurements for a Liebeck LA2573A airfoil at Reynolds numbers from 2.35×10^5 to 5×10^5. Their results showed that the peak frequency of the velocity spectra measured in the separated region agreed with the most amplified frequency predicted by a linear stability analysis of the inflectional velocity profiles across the separated shear layer.

Zaman et al.[13] conducted an experimental and numerical study of an LRN(1)-1007 airfoil near stalled conditions at chord Reynolds number of 7.5×10^4. Fluctuation velocity spectra clearly showed the existence and the significance of the dominant instability wave. Vortex shedding from the main separation was demonstrated by smoke-wire flow visualization. The complementary numerical study demonstrated that the measured low-frequency oscillation was a result of vortex shedding from the laminar separation bubble. The unsteady separation was observed to be nearly two dimensional along most of the wing span except near the wing tips.

Large-scale unsteadiness within the laminar separation bubble has also been observed in numerical simulations. The steady computations of Briley[14] found that a steady solution was not possible for strong adverse pressure gradient cases. He attributed the unsteadiness to a physical phenomenon and not to numerical instabilities. The triple-deck analysis used by Stewartson et al.[15] and Elliott and Smith[16] also could not obtain a steady separation solution for sufficiently strong adverse pressure gradient. Gruber et al.[17] and Bestek et al.[18] showed that the separation bubble becomes unsteady if a strong external pressure gradient is applied. Vortex shedding from the laminar separation bubble on an airfoil was computationally observed by Sugavanam and Wu[19] and Rumsey.[20] Ghia and Ghia[21] and Stremel[22] found a similar vortex-shedding process under conditions of airfoil stall. In some numerical studies, investigators found that the results were dependent on the turbulence model used. A detailed comparison of turbulence models applied to separated flows was considered by Rumsey and Vatsa.[23]

Pauley et al.[10] and Ripley and Pauley[11] performed numerical studies of the two-dimensional separation of a laminar flat plate boundary layer under the influence of an adverse pressure gradient. For a relatively weak adverse pressure gradient they observed a separated region that contained a steady closed separation bubble. When a stronger adverse pressure gradient was applied, a limit-cycle oscillation formed in which periodic vortex shedding occurred. The Strouhal number based on boundary-layer momentum thickness at separation was found to be independent of Reynolds number. The Strouhal number, however, was found to vary with the pressure coefficient distribution. The shedding frequency was determined by an inviscid linear stability analysis to be the most amplified instability wave of the shear layer. The computed time-averaged surface pressure distribution showed a region of nearly constant pressure followed by an abrupt decrease in surface pressure just before reattachment. The study of Ripley and Pauley applied the flow conditions of Gaster.[24] The time-averaged pressure distribution from the computational results compared closely with the experimental measurements of Gaster. In the absence of a third dimension and turbulence modeling, this investigation strongly confirms that two-dimensional vortex shedding is responsible for the formation of the low-Reynolds-number separation.

III. Numerical Scheme

The INS2D code, developed by Rogers and Kwak,[25] is adopted and then modified to conduct the present numerical experiments. The INS2D code solves the unsteady incompressible Navier–Stokes equations using the method of artificial compressibility as described by Rogers and Kwak.[25] Modifications to the INS2D code for the present study include the use of a generalized normal momentum equation for the pressure boundary and the use of an overlap procedure to update the calculated variables on the wake cut line.

A C-type mesh, produced by a hyperbolic grid generator based on Kinsey and Barth,[26] is employed in the present airfoil computation. The grid contains 425 points wrapped over the airfoil and 101 points normal to the airfoil. The computational domain extends to 15 chord lengths in all directions.

Extensive numerical experiments for the Eppler 387 airfoil at Reynolds number of 1×10^5 and 4-deg angle of attack were performed and documented in Lin.[27] Several observations, which are critical to the following computations, were obtained from the numerical experiments. It was found that the low-frequency oscillation as a result of the reflection of numerical noise from a smaller computational domain was eliminated by extending the computational domain to 15 chord lengths away from the airfoil surface. Grid resolution studies showed that the high-velocity-gradient regions about the leading edge and primary separation required increased grid clustering. A grid-independent smooth solution was obtained when at least 40 grid points were used in the normal direction across the primary separation region and no less than 60 uniform grid points were applied from the separation point to the reattachment point. By halving the time step in a series of computations, it was found that 150 time step intervals in one vortex-shedding cycle adequately resolved the cyclic behavior. The magnitude of the compressibility factor was found to have profound influence on the unsteady incompressible solution and played a critical role in the computational efficiency. A compressibility factor of 1000 at a Reynolds number of 1×10^5 produced a solution independent of the compressibility factor within a reasonable computation time. Furthermore, the optimum magnitude of the compressibility factor was analytically determined to be inversely proportional to the Reynolds number.

IV. Limit-Cycle Shedding

All computations were started from freestream conditions and without any perturbation. The computations were continued until the initial transients had decayed and limit-cycle shedding was asymptotically reached. The resulting limit-cycle vortex shedding is examined using instantaneous streamlines and vorticity contours. Streamwise velocity histories are recorded at several locations where vortex shedding and propagation occur.

A. Base Case at Reynolds Number = 1×10^5 and Angle of Attack = 4 deg

Results for the base case at 1×10^5 chord Reynolds number and 4-deg angle of attack are presented in detail to demonstrate flow characteristics common to all cases studied. For all Reynolds numbers considered, the limit-cycle streamwise velocity histories upstream of vortex shedding, downstream of vortex shedding, and downstream of vortex pairing clearly demonstrate that only one dominant frequency and its first and second subharmonic components are present.

The instantaneous streamlines of the limit-cycle shedding at 1×10^5 chord Reynolds number are shown in Fig. 2 for 10 equally spaced intervals. Two cycles of the periodic shedding as a result of the presence of vortex pairing are shown. A counter-rotating vortex within the leading primary separation grows to a critical size and eventually divides the primary separation into two distinct cells with the shed vortex moving downstream and the remaining primary separation regrowing. Vortex pairing, one of the major mechanisms responsible for the shear layer growth, was also observed. A similar shedding structure was found in Pauley et al.[10] and Ripley and Pauley.[11]

It can be seen from the streamline contours that the flow near the separation point is virtually steady. A slight fluctuation in the streamline contours above the counter-rotating region indicates the

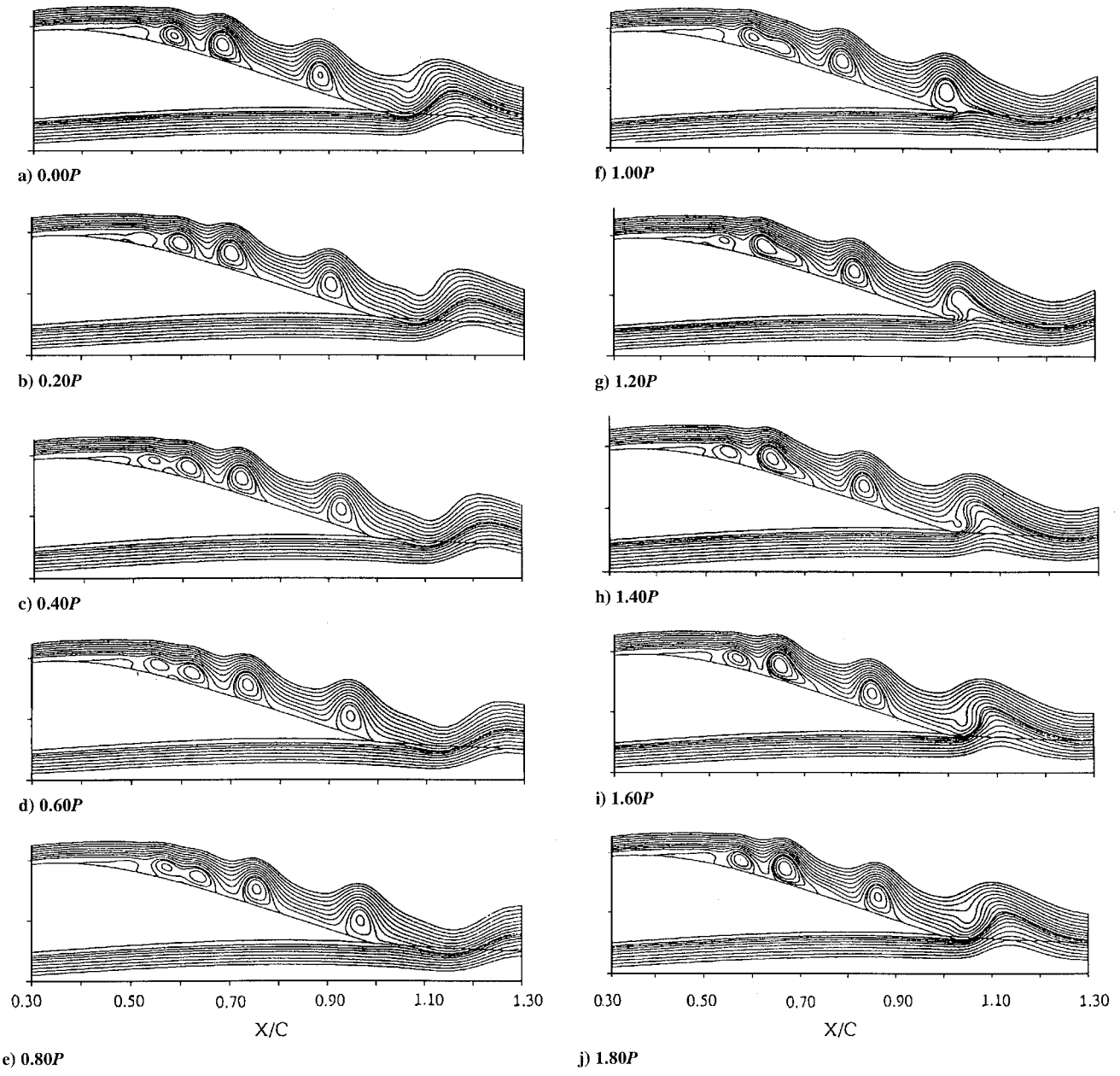

Fig. 2 Streamlines for limit-cycle shedding at $Re = 1 \times 10^5$ and 4-deg angle of attack (P = period).

entrainment of higher-momentum fluid. The most significant entrainment occurs as the vortex is being shed. This entrainment facilitates the continuation of the vortex shedding and can be regarded as a reattachment mechanism that serves a role similar to the familiar turbulent mixing.

Vortex pairing begins at a phase of $0.40P$, as shown in Fig. 2c. Between $X/C = 55$ and 60%, neighboring pairs of vortices are seen to roll around each other. Viscous diffusion smears out the identities of individual vortices to leave a single, larger vortex where originally there were two. The coalesced vortices then significantly increase the boundary-layer thickness downstream of the vortex pairing. The significant increase of the boundary-layer thickness as a result of vortex pairing found in the present study is consistent with the observations of the wake study of Winant and Browand.[28] In their study, vortex pairing was responsible for the rapid growth of the free shear layer. The vortex pairing is believed to be induced by the adverse pressure gradient, which decelerates the leading vortex; the trailing vortex reaches the leading vortex and the two vortices merge. The vortex propagation velocity is found to be about 60% of the local freestream velocity. In the flat plate studies of Pauley et al.[10] and Ripley and Pauley,[11] convection velocities of the shed vortices were also found to be at about 60% of the local freestream velocities.

To better understand the shedding process and the subsequent vortex motions, the negative vorticity in Fig. 3b (corresponding to $0.6P$ in Fig. 2) can be examined. Near the separation point the shear layer lifts away from the surface. As unstable waves grow, the shear layer rolls up into discrete vortical structures. As a vortex travels downstream, the vorticity strength is attenuated under the action of viscous diffusion. As first pointed out by Pauley et al.,[10] the observed vortex formation and propagation strikingly resemble the more familiar free shear flows of Winant and Browand[28] and Scott.[29]

B. Reynolds Number Effect

For a fixed 4-deg angle of attack, computations are conducted at chord Reynolds numbers of 6×10^4, 1×10^5, and 2×10^5. Although the vortex-shedding mechanism occurs at all Reynolds numbers examined, a decrease in Reynolds number causes the viscous effect to become stronger, resulting in a greater boundary-layer thickness as seen in Fig. 3. At lower Reynolds number, a larger main separation region forms, and the subsequent shed vortices are larger.

For the case of $Re = 6 \times 10^4$, vortex pairing takes place at two locations downstream of vortex shedding. The beginning of the first pairing occurs at $X/C = 58\%$. The two individual vortices roll around each other and move downstream. While these

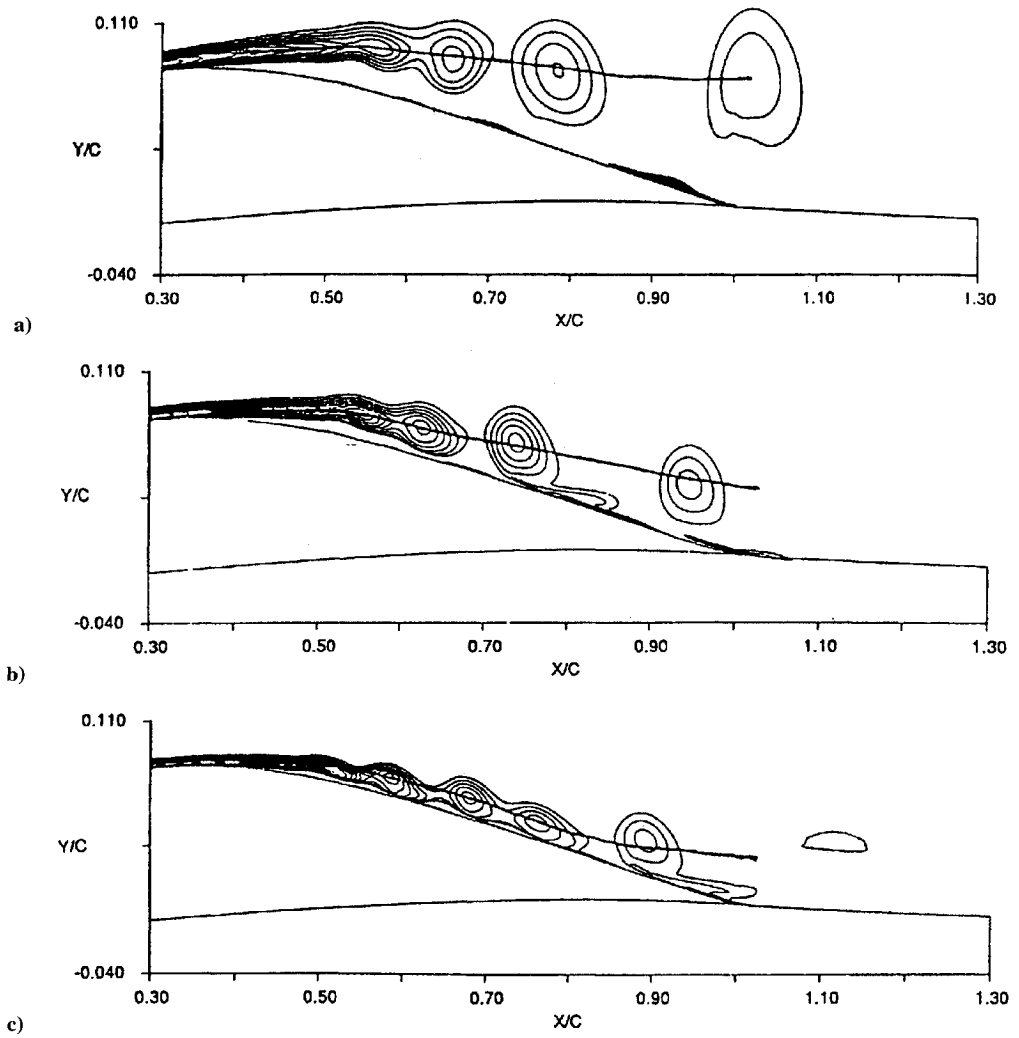

Fig. 3 Vorticity contours and vortex trajectory for angle of attack of 4 deg and Re = a) 6×10^4, b) 1×10^5, and c) 2×10^5.

coalesced vortices continue to travel downstream, two more vortices are shed at $X/C = 51\%$ and pair at $X/C = 58\%$. The newly formed composite vortex will eventually catch up with the earlier formed composite vortex. The onset of this second pairing is at $X/C = 86\%$. Because there are two pairings, when the vortex structure reaches the airfoil trailing edge, it consists of four originally individual vortices that have coalesced. The multiple vortex pairings cause the boundary-layer thickness at the trailing edge to be greater for the low-Reynolds-number case. Similar to the base case at $Re = 1 \times 10^5$, only one vortex pairing occurs when $Re = 2 \times 10^5$. For this higher Reynolds number, the vortex shedding takes place at $X/C = 45\%$, and the only vortex pairing occurs at $X/C = 76\%$.

In Fig. 3, vortex trajectories for the three Reynolds numbers are charted by following the vortex center of a typical vortex. The vortex center is defined as the vorticity center of a shed vortex. The marked solid line in each figure is the journey of a typical shed vortex. After shedding from the primary separation, the vortices are lifted away from the surface and initially travel along the straight line described by the separation angle. When vortex pairing occurs, the trajectory curves back to a line that is nearly parallel to the surface. Since the airfoil turns away from the boundary layer, the shed vortex moves away from the airfoil surface near the trailing edge. The vortex center, which describes the associated vortex trajectory, is located approximately at the lower edge of the free shear layer. At lower Reynolds numbers, the vortex trajectory follows a higher course, and the free shear layer is displaced farther from the airfoil surface.

C. Angle-of-Attack Effect

For a fixed chord Reynolds number of 1×10^5, the angle-of-attack effect on the limit-cycle shedding is investigated by cases at 0-, 4-, and 7-deg angle of attack. Shear layer lifting near the separation point, vortex roll-up, and vortex pairing can be realized by negative vorticity contours, as shown in Figs. 3b and 4.

Vortex trajectories for the three angles of attack are charted in the figures by following the vortex center. For all cases, the vortices are lifted away from the surface initially and follow along the straight line described by the separation angle. The location of the separation point, however, moves upstream when the angle of attack is increased. Higher-momentum fluid is entrained to facilitate the continuation of the vortex shedding, which takes place at $X/C = 57$ and 38% for 0- and 7-deg angle of attack, respectively. When vortex pairing occurs, the trajectory curves back to a line that is nearly parallel to the surface. Changes in the locations of separation and vortex shedding as a result of angle of attack produce differences in the upstream portions of the three vortex trajectories. The downstream portions of the vortex trajectories, however, are nearly identical.

V. Shedding Frequency and Shear Layer Instability

In the absence of the high-frequency harmonics, the dominant shedding frequency can easily be found from the velocity histories. A Strouhal number based on the global quantities is defined as

$$Sr_C = fC/U_\infty \tag{1}$$

Following Pauley et al.[10] and Ripley and Pauley,[11] a Strouhal number based on the local quantities at the separation point is defined as

$$Sr_\theta = \frac{f\theta_{\text{sep}}}{U_{\text{sep}}} \tag{2}$$

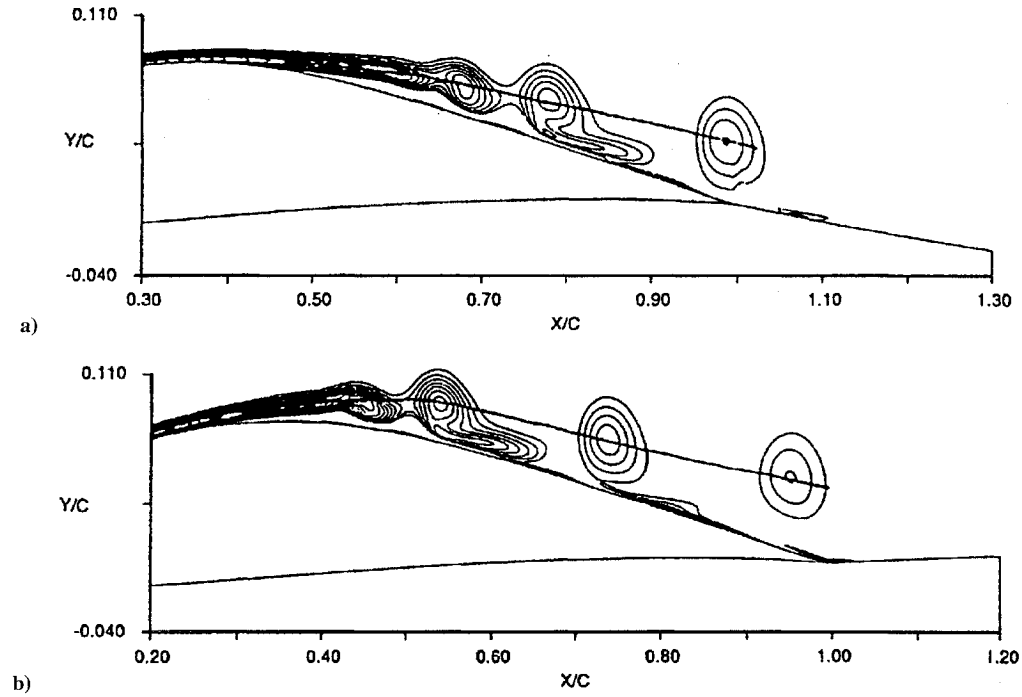

Fig. 4 Vorticity contours and vortex trajectory for $R = 1 \times 10^5$ and angle of attack: a) 0 and b) 7 deg.

Table 1 Vortex-shedding frequency

Reynolds no.	Angle of attack, deg	U_{scp}/U_∞	θ_{scp}/C	Sr_C	Sr_θ
6×10^4	4	1.010	0.00131	4.30	0.00558
1×10^5	4	0.932	0.00121	5.11	0.00663
2×10^5	4	0.925	0.00118	4.80	0.00612
1×10^5	0	0.874	0.00149	4.67	0.00796
1×10^5	7	1.012	0.00107	5.46	0.00577

The global separation characteristics for the five cases investigated are listed in Table 1.

The present computations do not show a clear collapse of Sr_C or Sr_θ. This differs from the findings of Pauley et al.[10] and Ripley and Pauley.[11] In each of those previous studies, Sr_θ was found to collapse for all Reynolds numbers and pressure gradient strengths investigated. The characteristic value of Sr_θ, however, was different in the two studies. Each of those previous studies considered laminar boundary-layer separation on a flat plate as a result of an externally applied pressure gradient. The adverse pressure gradient was locally applied and each study considered one general shape for C_P. According to Ripley and Pauley, differences in the applied pressure gradient distribution of the two studies resulted in a different characteristic Sr_θ. This reasoning also explains why there is no collapse in Strouhal number for the present study. When the boundary-layer development occurs on an airfoil, both angle of attack and Reynolds number cause variations in the C_P distribution.

Linear stability theory has been extremely successful in predicting many essential features of the initial development of a variety of flow instabilities. The instability mechanism that causes the vortex shedding is investigated here using linear stability theory. It has been known that the velocity profile possesses an inflection point downstream of separation. According to linear stability theory, an inviscid type of instability wave (Kelvin–Helmholtz instability wave) might arise as a result of the inflectional profile. If this inflectional velocity profile occurs in free shear layers, e.g., wakes, mixing layers, and jets, the oscillations as a result of the inviscid instability amplify rapidly out of the linear range and often to lead to turbulence.[30] However, because of the stabilizing viscous effect of the neighboring wall and the low Reynolds number, the separated boundary layer may remain laminar and the instability result in vortex shedding without transition.[30] The oscillatory motion would then show one single dominant component that produces the vortex shedding. This limit-cycle oscillation resulting from vortex shedding has been convincingly demonstrated by the periodic variation in the local streamwise velocities and the global aerodynamic coefficients C_L and C_D.

As noted by Pauley et al.,[10] the vorticity distribution in the separated boundary layer is similar to that of a mixing layer. Therefore the stability characteristics of the present unsteady separation can be determined using the stability analysis of a mixing layer by Michalke.[31,32] The shear layer is described by the vorticity layer δ_ω and the velocity ratio VR, which are defined as

$$\delta_\omega = \frac{\Delta U}{(\delta u/\delta y)_{\max}} \tag{3}$$

$$VR = \frac{\Delta U}{2U_{\text{avg}}} \tag{4}$$

where $\Delta U = U_2 - U_1$ and $U_{\text{avg}} = \frac{1}{2}(U_1 + U_2)$. The terms U_1 and U_2 are the freestream velocities across the mixing layer. Michalke found the most amplified frequency to correspond to

$$f^* = (\delta_\omega/4)(2\pi f/U_{\text{avg}}) \approx 0.21 \tag{5}$$

A recent study by Huerre and Monkewitz[33] determined that Michalke's spatial stability analysis is only valid when the velocity ratio VR is less than 1.315.

For the present study, the time-averaged velocity profiles within each separation bubble are used to determine f^*. The leading part of the bubble contains virtually stagnant fluid, corresponding to $VR \approx 1.0$. Therefore Eq. (5) can be used in the present situation. Upstream of the time-averaged vortex center, the frequency parameter for the five cases studied was found to be $f^* = 0.208 \pm 1.01\%$. The favorable comparison with Eq. (5) indicates that the vortex shedding is a result of the inviscid instability of the inflectional velocity profile downstream of the separation point. In the downstream region of the time-averaged vortex center, however, f^* varies since the presence of vortex shedding has modified the time-averaged velocity profile.

VI. Time-Averaged View of the Separation

The inherently time-averaged results from the Eppler 387 airfoil tests by McGhee et al.[12] were compared with the present results.

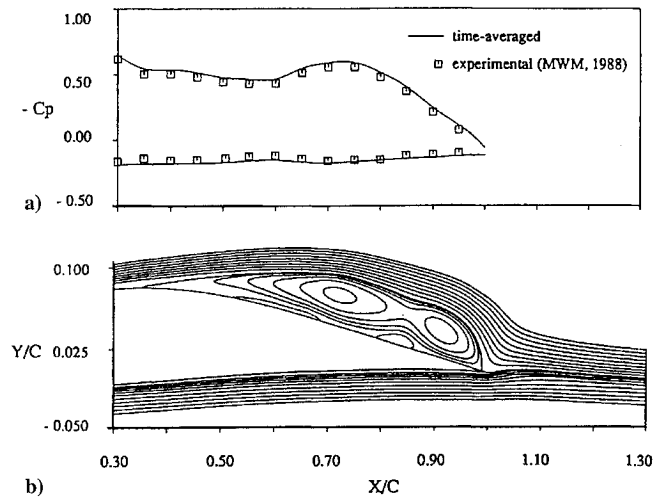

Fig. 5 Time-averaged separation bubble for $Re = 6 \times 10^4$ and angle of attack of 4 deg: a) pressure coefficient and b) streamlines.

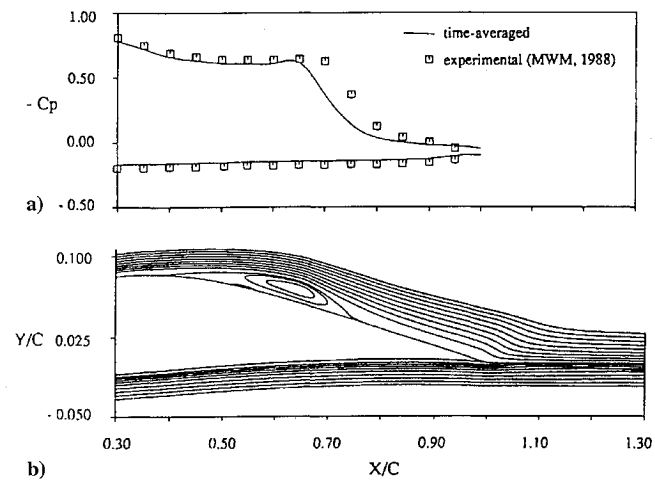

Fig. 6 Time-averaged separation bubble for $Re = 1 \times 10^5$ and angle of attack of 4 deg: a) pressure coefficient and b) streamlines.

To facilitate comparison, the present computed unsteady results are time averaged over an even number of shedding cycles. An even number of shedding periods is used because of the presence of vortex pairing and the subsequent period doubling.

A. Aerodynamic Coefficients

Similar to the streamwise velocity histories, the computed time-dependent lift coefficient C_L and drag coefficient C_D show cyclic behavior reflecting periodic shedding. The average relative amplitude of C_L and C_D oscillations for the five cases studied is found to be 25 and 45%, respectively. In Table 2, the computed time-averaged C_L and C_D are compared with the experimental results of McGhee et al.[12] No more than 2.0% relative error of C_L and 8.0% relative error of C_D are found.

B. Time-Averaged Bubbles

Time-averaged C_P distribution and streamline contours are shown in Figs. 5–9 for the five cases studied. In all time-averaged C_P distribution plots, experimental data of McGhee et al.[12] in chord coordinates are also included to enable close comparison. For the five cases investigated, the time-averaged C_P distribution of McGhee et al. is well predicted by the present computed time-averaged results.

The time-averaged separation bubble displays characteristics similar to the conventional steady transitional separation bubble. Near the separation point, slow moving fluid is present in the separated region and the surface pressure is nearly uniform. However, in the trailing region of the bubble, a strong recirculation is present and

Table 2 Time-averaged aerodynamic coefficients for present computations and McGee et al.[12] (noted as MWM)

Reynolds no.	Angle of attack, deg	$C_{L,\text{avg}}$	$C_{L,\text{MWM}}$	$C_{L,\text{error}}$, %	$C_{D,\text{avg}}$	$C_{D,\text{MWM}}$	$C_{D,\text{error}}$, %
6×10^4	4	0.656	0.643	2.0	0.0463	0.0431	7.4
1×10^5	4	0.793	0.778	1.9	0.0248	0.0230	7.8
2×10^5	4	0.800	0.785	1.9	0.0142	0.0133	6.8
1×10^5	0	0.388	0.390	0.5	0.0182	0.0173	5.2
1×10^5	7	1.052	1.072	1.9	0.0228	0.0211	8.0

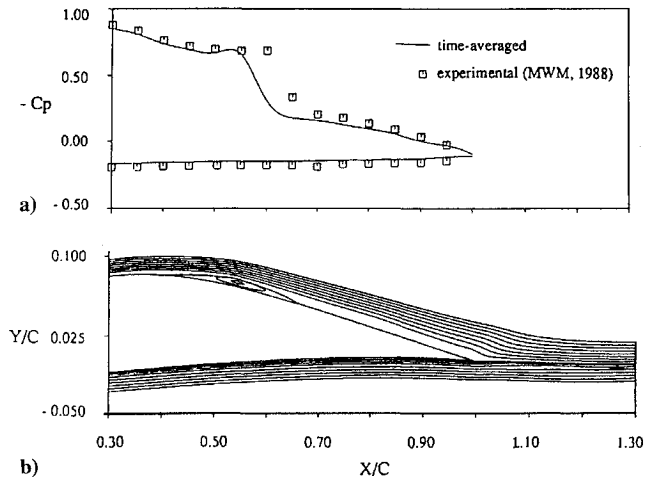

Fig. 7 Time-averaged separation bubble for $Re = 2 \times 10^5$ and angle of attack of 4 deg: a) pressure coefficient and b) streamlines.

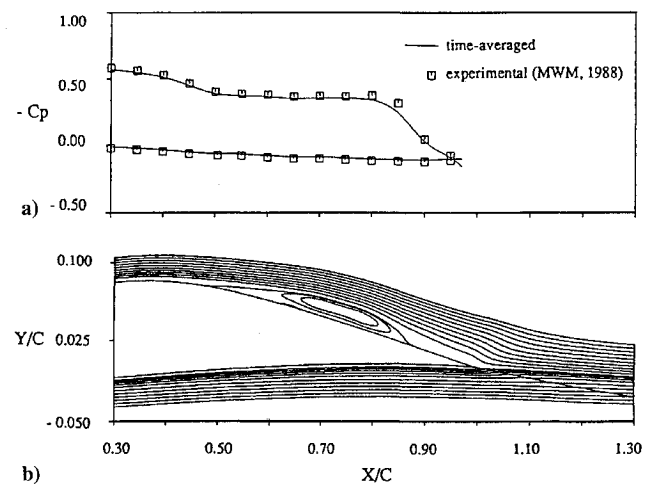

Fig. 8 Time-averaged separation bubble for $Re = 1 \times 10^5$ and angle of attack of 0 deg: a) pressure coefficient and b) streamlines.

corresponds to the region of strong pressure gradient. By comparison of Figs. 5b, 6b, and 7b, it is seen that the time-averaged bubble length and height decrease with increasing Reynolds number. Increasing angle of attack causes boundary-layer separation to occur further upstream and produce a shorter time-averaged separation bubble, as shown in Figs. 8b, 6b, and 9b. In the absence of turbulence, the shorter bubble length associated with higher angle of attack can be attributed to the increased separation angle of the resulting free shear layer. Since the free shear layer at higher angle of attack is less confined by the neighboring airfoil surface, the boundary layer is more unstable and vortex shedding takes place earlier and more vigorously, resulting in a shorter time-averaged separation bubble. The Reynolds-number effect and angle-of-attack effect on the time-averaged separation bubble are similar to their respective effects on the corresponding unsteady separated flowfields, which have been described in Sec. IV.

Table 3 Separation point (SP), reattachment point (RP), and bubble length (BL) for present computations and McGhee et al.[12] (noted as MWM); NR = not reported

Reynolds no.	Angle of attack, deg	SP	RP	BL	SP_{MWM}	RP_{MWM}	BL_{MWM}
6×10^4	4	0.345	0.957	0.612	NR	NR	NR
1×10^5	4	0.355	0.762	0.407	0.35	0.73	0.38
2×10^5	4	0.407	0.662	0.255	0.40	0.62	0.22
1×10^5	0	0.452	0.885	0.433	0.45	0.87	0.42
1×10^5	7	0.288	0.635	0.347	0.32	0.56	0.24

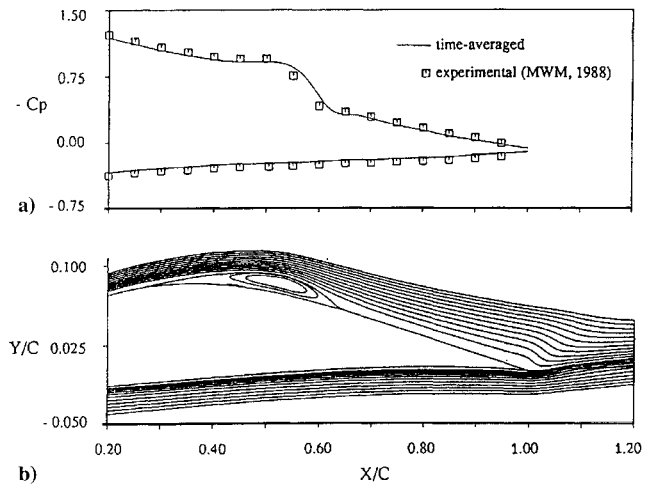

Fig. 9 Time-averaged separation bubble for $Re = 1 \times 10^5$ and angle of attack of 7 deg: a) pressure coefficient and b) streamlines.

The laminar separation point, reattachment point, and bubble length measured as a fraction of the chord length are summarized in Table 3 for the current time-averaged results and the experimental measurements of McGhee et al.[12] In all but the highest angle-of-attack case, the experimental separation point, reattachment point, and bubble length are faithfully reproduced by the present computations. It is not understood why the computed time-averaged bubble length for the case of 7-deg angle of attack is longer than that observed experimentally. Noting that the experimental separation location occurred further downstream than the computed separation location, the present authors hypothesize that the experimental freestream turbulence levels, ranging from 0.06 to 0.16%, influenced the bubble development. Freestream turbulence has been known to delay separation and at the same time accelerate transition of the separated shear layer. The net effect of high freestream turbulence is a delayed separation and an early reattachment, therefore a shorter bubble. In addition, note that the separation point and bubble length measured by McGhee et al.[12] are very sensitive to small changes in angle of attack when the Eppler 387 airfoil is at high angle of attack. This sensitivity at high angle of attack could also explain the discrepancies between the present computed results and the wind-tunnel results at 7-deg angle of attack.

VII. Conclusions

The unsteady large-scale boundary-layer separation characteristics were studied for an Eppler 387 airfoil at several angles of attack and Reynolds numbers. For all cases studied, laminar boundary-layer separation on the airfoil surface resulted in periodic vortex shedding and subsequent pairing downstream. The vortex shedding was caused by the dominant inviscid instability wave induced by the inflection velocity profile downstream of the separation point. Time averaging the computed unsteady structure resulted in a separation bubble that was strikingly similar to the conventional laminar separation bubble. The time-averaged results of the computations showed a region of nearly uniform surface pressure followed by an abrupt increase in surface pressure just before reattachment. The favorable comparison between the computed time-averaged results and previous experimentally measured results suggests that two-dimensional large-scale structures, in the form of vortex shedding, control the laminar separation bubble and the omnipresent small-scale turbulence plays only a secondary role. The universality of the unsteady large-scale structure previously found on a flat plate is confirmed through the present low-Reynolds-number airfoil computations. Increasing Reynolds number reduced the unsteady main separation region, moved the separation point downstream, reduced the separation angle, and shortened the time-averaged separation bubble. Increasing angle of attack moved the separation point upstream and shortened the time-averaged separation bubble.

Acknowledgments

This research has been supported by the U.S. Office of Naval Research under Contract N00014-90-J-1169 monitored by Edwin P. Rood. Computational facilities were provided by the NAVOCEANO Primary Oceanographic Prediction System and the Pittsburgh Supercomputing Center. These contributions are gratefully acknowledged.

References

[1]Carmichael, B. H., "Low Reynolds Number Airfoil Survey," Vol. 1, NASA CR 165803, Nov. 1981.

[2]Miley, S. J., "A Catalog of Low Reynolds Number Airfoil Data for Wind Turbine Applications," Aerospace Engineering Dept., Texas A&M Univ., College Station, TX, Feb. 1982.

[3]Lissaman, P. B. S., "Low-Reynolds-Number Airfoils," *Annual Review of Fluid Mechanics*, Vol. 12, 1983, pp. 255–280.

[4]Mueller, T. J., "Low Reynolds Number Vehicles," AGARDograph 288, Feb. 1985.

[5]Brendel, M., and Mueller, T. J., "Transition Phenomena on Airfoils Operating at Low Chord Reynolds Numbers in Steady and Unsteady Flow," *Numerical and Physical Aspects of Aerodynamic Flows IV*, edited by T. Cebeci, Springer–Verlag, New York, 1990, pp. 333–344.

[6]Brendel, M., and Mueller, T. J., "Boundary Layer Measurements on an Airfoil at a Low Reynolds Numbers in an Oscillating Freestream," *AIAA Journal*, Vol. 26, No. 3, 1988, pp. 257–263.

[7]Horton, H. P., "A Semi-Empirical Theory for the Growth and Bursting of Laminar Separation Bubbles," *Aeronautical Research Council Current Papers*, CP 1073, Univ. of London, 1967.

[8]Brendel, M., and Mueller, T. J., "Boundary Layer Measurements on an Airfoil at Low Reynolds Numbers," *Journal of Aircraft*, Vol. 25, No. 7, 1988, pp. 612–617.

[9]LeBlanc, P., Blackwelder, R., and Liebeck, R., "A Comparison Between Boundary Layer Measurements in a Laminar Separation Bubble Flow and Linear Stability Theory Calculations," *Perspectives in Turbulence Studies*, edited by H. U. Meier and P. Bradshaw, Springer–Verlag, New York, 1987, pp. 189–205.

[10]Pauley, L. L., Moin, P., and Reynolds, W. C., "The Structure of Two-Dimensional Separation," *Journal of Fluid Mechanics*, Vol. 220, Nov. 1990, pp. 397–411.

[11]Ripley, M. D., and Pauley, L. L., "The Unsteady Structure of Two-Dimensional Steady Laminar Separation," *Physics of Fluids A*, Vol. 5, No. 12, 1993, pp. 3099–3106.

[12]McGhee, R. J., Walker, B. S., and Millard, B. F., "Experimental Results for the Eppler 387 Airfoil at Low Reynolds Numbers in the Langley Low-Turbulence Pressure Tunnel," NASA TM 4062, Oct. 1988.

[13]Zaman, K. B. M. Q., McKinzie, D. J., and Rumsey, C. L., "A Natural Low-Frequency Oscillation of the Flow over an Airfoil Near Stalling Conditions," *Journal of Fluid Mechanics*, Vol. 202, May 1989, pp. 403–442.

[14]Briley, W. R., "A Numerical Study of Laminar Separation Bubbles Using the Navier–Stokes Equations," *Journal of Fluid Mechanics*, Vol. 47, Pt. 4, 1971, pp. 713–736.

[15]Stewartson, K., Smith, F. T., and Kaups, K., "Marginal Separation," *Studies in Applied Mathematics*, Vol. 67, No. 1, 1982, pp. 45–61.

[16]Elliott, J. W., and Smith, F. T., "Dynamic Stall Due to Unsteady Marginal Separation," *Journal of Fluid Mechanics*, Vol. 179, June 1987, pp. 489–512.

[17]Gruber, K., Bestek, H., and Fasel, H., "Interaction Between a Tollmien-Schlichting Wave and a Laminar Separation Bubble," AIAA Paper 87-1256, June 1987.

[18]Bestek, H., Gruber, K., and Fasel, H., "Self-Excited Unsteadiness of Laminar Separation Bubbles Caused by Natural Transition," *The Prediction and Exploitation of Separated Flow*, Royal Aeronautical Society, 1989.

[19]Sugavanam, A., and Wu, J. C., "Numerical Study of Separated Turbulent Flow over Airfoils," *AIAA Journal*, Vol. 20, No. 4, 1980, pp. 464–470.

[20]Rumsey, C. L., "A Computational Analysis of Flow Separation over Five Different Airfoil Geometries at High Angles-of-Attack," AIAA Paper 87-0188, Jan. 1987.

[21]Ghia, K. N., and Ghia, U., "Direct Solution Techniques for Viscous Flow and Their Control," U.S. Air Force Office of Scientific Research, AFOSR-TR-91-0531, May 1991.

[22]Stremel, P. M., "The Effect of Reynolds Number and Turbulence on Airfoil Aerodynamics at −90 Degrees Incidence," AIAA Paper 93-0206, Jan. 1993.

[23]Rumsey, C. L., and Vatsa, V. N., "A Comparison of the Predictive Capabilities of Several Turbulence Models Using Upwind and Central-Difference Computer Codes," AIAA Paper 93-0192, Jan. 1993.

[24]Gaster, M., "The Structure and Behavior of Laminar Separation Bubbles," AGARD Conf. on Separated Flow, AGARD CP-4, 1966, pp. 813–854.

[25]Rogers, S. E., and Kwak, D., "An Upwind Differencing Scheme for the Incompressible Navier–Stokes Equations," *Applied Numerical Mathematics*, Vol. 8, No. 1, 1991, pp. 43–64.

[26]Kinsey, D. W., and Barth, T. J., "Description of a Hyperbolic Grid Generating Procedure for Arbitrary Two-Dimensional Bodies," U.S. Air Force Wright Aeronutical Lab., AFWAL-TM 84-191, July 1984.

[27]Lin, J. C. M., "Numerical Investigation of the Large-Scale Structure in Laminar Separation Bubbles," Ph.D. Thesis, Dept. of Mechanical Engineering, Pennsylvania State Univ., University Park, PA, 1993.

[28]Winant, C. D., and Browand, F. K., "Vortex Pairing: The Mechanism of Turbulent Mixing-Layer Growth at Moderate Reynolds Number," *Journal of Fluid Mechanics*, Vol. 63, Pt. 2, 1974, pp. 237–255.

[29]Scott, J. N., "Numerical Simulation of Self-Sustained and Forced Oscillations in Jet Shear Layers," *Forum on Unsteady Flow Separation*, edited by K. N. Ghia, ASME FED-Vol. 52, American Society of Mechanical Engineers, New York, 1987, pp. 123–130.

[30]Morkovin, M. V., "Flow Around Circular Cylinder—A Kaleidoscope of Challenging Fluid Phenomena," *Symposium on Fully Separated Flows*, edited by A. G. Hansen, Fluids Engineering Div. Conf., American Society of Mechanical Engineers, New York, 1964, pp. 102–118.

[31]Michalke, A., "On the Inviscid Instability of the Hyperbolic-Tangent Velocity Profile," *Journal of Fluid Mechanics*, Vol. 19, Pt. 4, 1964, pp. 543–556.

[32]Michalke, A., "On Spatially Growing Disturbances in an Inviscid Shear Layer," *Journal of Fluid Mechanics*, Vol. 23, Pt. 3, 1955, pp. 521–544.

[33]Huerre, P., and Monkewitz, P. A., "Absolute and Convective Instabilities in Free Shear Layers," *Journal of Fluid Mechanics*, Vol. 159, Oct. 1985, pp. 151–168.